# Synchronization of a Multistatic High Resolution Imaging Radar using Low-Cost Satellite TV Receiver Hardware


Fabian Hochberg
*Microwaves and Radar Institute*
*German Aerospace Center (DLR)*
Weßling, Germany
Email: fabian.hochberg@dlr.de

Matthias Jirousek
*Microwaves and Radar Institute*
*German Aerospace Center (DLR)*
Weßling, Germany
Email: matthias.jirousek@dlr.de

Simon Anger
*Microwaves and Radar Institute*
*German Aerospace Center (DLR)*
Weßling, Germany
Email: simon.anger@dlr.de

Markus Peichl
*Microwaves and Radar Institute*
*German Aerospace Center (DLR)*
Weßling, Germany
Email: markus.peichl@dlr.de

Thomas Zwick
*Institute of Radio Frequency*
*Engineering and Electronics*
*Karlsruhe Institute of Technology (KIT)*
Karlsruhe, Germany
Email: thomas.zwick@kit.edu



***Abstract*—With growing interest in multistatic radar systems, the need for accurate and precise synchronization schemes become increasingly important. Large baseline systems face substantial challenges to achieve the required synchronization accuracy. In this work, we present a synchronization technique applicable for high resolution imaging radar systems based on the reception of a wide bandwidth broadcast TV signal at remote receive-only nodes and at the transmitting and receiving base node. Coherence is then established using signal processing in the post-processing stages to regain the timing and phase differences present between the participating nodes. This allows to greatly increase the synchronization accuracy in terms of timing and oscillator phase tracking compared to conventional GNSS based synchronization schemes. It is independent of the number of participating nodes, and we demonstrate a standard deviation phase noise in X band as low as 1.69° and timing jitters as low as 2.42 ps allowing high resolution SAR / ISAR techniques to be employed. It is verified using real-world measurements with modified consumer COTS LNBs to receive the satellite TV signal.**



***Index Terms*—ISAR, multistatics, synchronization, timing.**


## I. Introduction

Recent years have shown an increasing interest in multistatic sensor systems and multistatic imaging radar [1]–[4]. A key challenge for such systems is the synchronization scheme employed, which may take up considerate hardware resources. A common approach is to use a line-of-sight (LOS) communication or ranging link to track the location, timing and oscillator phase of multiple remotes [3]–[7]. In the case of large baseline systems, such as the experimental multistatic space surveillance system IoSiS-NG (Imaging of Satellites in Space – Next Generation, [8]), this approach becomes unfeasible, as large baseline separation hinder LOS propagation. To coherently image objects in space using a multitude of spatially separated receivers, we investigate synchronization schemes that enhance the achievable accuracy beyond the well-known solution by oscillator disciplining via global navigation satellite systems (GNSSs). Exceptionally, when operating at higher frequencies than the GNSS signals, phase coherence becomes very difficult or impossible to achieve.

As a first research result, the work presented here uses a GNSS-disciplined base clock in a radar system operating in X band and exploits non-cooperative (NC) signals arriving at all locations participating in the sensor network. As a proof-of-concept we aimed to use the broadcast satellite television (TV) signals from the ASTRA geostationary satellites located at 19.2° East with a down link frequency in the European $K_u$ band (11.7 GHz to 12.5 GHz) [9]. In the post-processing stage, the identical signal payload at all participating nodes can then be used to compare the signal from the receive-only remote nodes to the transmitting base node. The comparison in time, but more importantly in phase, of all receive-only nodes' TV signal to the base node's signal allows the extraction of time and phase offsets, which in turn are then applied to the received radar echos. Other works like [10]–[13] have also attempted synchronization and/or localization using NC signals, however we elevate this principle in our work to obtain a phase estimate to correct for the local oscillator (LO) phase needed for imaging radar applications, as only relative synchronization to the transmitter is needed.

We structured this paper as follows. In Section II we introduce the radar system concept as well as the theory behind the synchronization scheme. In Section III the hardware setup and modifications to consumer commercial off-the-shelf (COTS) low-noise block downconverters (LNBs) are explained, and measurements with real satellite signals are established. Lastly,


This work was supported by the Bavarian Ministry of Economic Affairs, Regional Development and Energy within the scope of the IoSiS-NG project.




**Article published by IEEE:** https://doi.org/10.1109/RadarConf2663773.2026.11675632
**Cite as:** F. Hochberg, M. Jirousek, S. Anger, M. Peichl and T. Zwick, "Synchronization of a Multistatic High Resolution Imaging Radar using Low-Cost Satellite TV Receiver Hardware," *2026 IEEE Radar Conference (RadarConf'26)*, Phoenix, AZ, USA, 2026, pp. 1-6, doi: 10.1109/RadarConf2663773.2026.11675632.

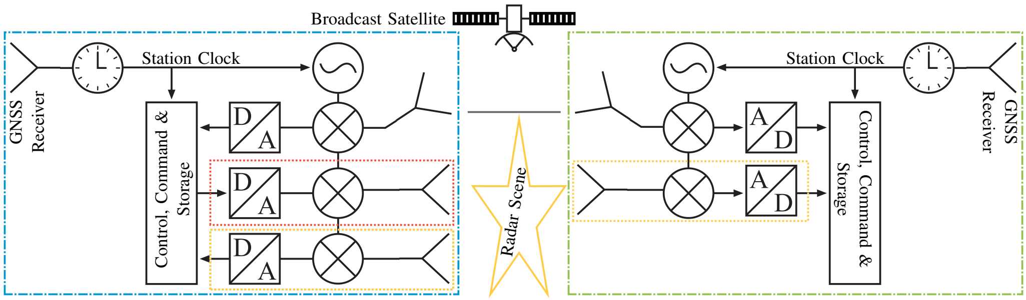


Fig. 1: Proposed system concept with a single monostatic radar node (base node; left-hand side in blue) and a receive-only remote node (right-hand side in green) of which a single node of arbitrary many is depicted. The receivers for the broadcast TV signals are at the top and the receivers for the radar echo are marked in yellow with the dotted box. The radar signal transmitter, which is only present at the base node, is marked with the red dotted box. The key to note is that both the radar signal and TV signal undergo the same frequency conversion.

in Section IV and V the discussion on the measurement data and a conclusion and outlook are given.

## II. System Introduction and Synchronization Scheme

In order to exploit the bi- or multistatic signatures of objects, distributed synchronized receivers are deployed over a multitude of baseline lengths. The aim of the system is to map objects in space and collect a more comprehensive amount of information than would be possible with a monostatic system. This acquisition geometry puts significant constraints on the employed synchronization scheme, as far baselines of dozens of kilometers are required to achieve a significant bistatic angle. With such constraints, most coherent synchronization schemes relying on a LOS link, such as [4], become unfeasible as no LOS propagation between the participating nodes is possible.

This work focuses on a frequency modulated pulse radar, as the time-domain sampling gives the needed flexibility to focus images in this challenging application with extraordinary resolution (up to 36 % relative bandwidth in X band). Pulsed data acquisition is thus also at the heart of this synchronization scheme, as the accuracy of the timing and phase estimation requires besides a sufficient signal-to-noise ratio (SNR) also a wide bandwidth [14, Chapter 3.11]. High bandwidth acquisitions are limited by the available technology in acquisition duration. Our system concept can be observed in Fig. 1.

Within each node the station clock ticks at the speed of the reference oscillator used within the node. When using GNSS disciplined oscillators, the median long term drift is zero and

$$\lim_{t\to\infty} \frac{1}{t} \int \frac{f_n^i(t)}{f_0} \,\mathrm{d}t = 1 \qquad (1)$$

holds. Here, $f_n^i$ is the time-varying instantaneous frequency of the oscillator at node $n$ and $f_0$ is its nominal frequency. The oscillator is monitored against the GNSSs time signal and steered via an active control loop, typically utilizing the pulse-per-second signal (PPS) signal [15]. This approach results in a relatively slow control loop response time, leaving short-term non-deterministic drift effects, such as temperature fluctuations and supply voltage variations, inherent to disciplined oscillators. For high resolution imaging tasks, this effect may not be neglected.

Moreover, the phase relationship from the base node to the remote nodes in the analog mixing stages in the context of (inverse) synthetic-aperture radar (SAR) is of uttermost importance. Unknown phase drifts heavily degrade the coherence between the received signals and thus hinder coherent multistatic imaging. When a phase-locked loop (PLL) is used to obtain the LO signal, uncorrelated phase noise and short term drift contributions outside the PLL's loop filter bandwidth are present and yet independent of the reference. This decorrelates the imaging signal and reduces the multistatic image quality. We propose a method for determining instantaneous time and phase differences by the reception of a TV signal at all participating nodes.

### *A. Satellite TV reception model*

The broadband transponder TV signal can be modeled with

$$s_{\mathrm{TV}}(t) = A \cdot \sum_{c=0}^{C} m_c(t) \cdot \exp(\mathrm{j}2\pi f_{c,\mathrm{sub}} t) \cdot \exp\left(\mathrm{j}2\pi f_{\mathrm{c}} t\right) , \qquad (2)$$

where $A$ is the signal's amplitude, $m_c(t)$ is the complex pulse-formed baseband modulation signal of subcarrier $c$ (of $C$ total carriers) at subcarrier baseband frequency of $f_{c,\mathrm{sub}}$ and the overall carrier frequency $f_{\mathrm{c}}$. This signal is received at all nodes and converted to baseband using a GNSS referenced LO signal. For the $n$-th node this received signal can be modeled with

$$\begin{aligned} r_n(t) = \; & D_n \cdot s_{\mathrm{TV}}(t-\tau_n) \\ & \exp\left(-\mathrm{j}\left(2\pi f_{n,\mathrm{LO}} t + \varphi_{n,0} + \varsigma_n(t)\right)\right) \\ & + w_n(t) \end{aligned} \qquad (3)$$

$$\text{with } \tau_n = \frac{\|\vec{x}_{\mathrm{sat}} - \vec{x}_n\|}{\mathrm{c}_0} ,$$

where $D_n$ is an amplitude attenuation due to losses and free-space propagation, $f_{n,\mathrm{LO}}$ is the LO signal frequency of node $n$, $\varphi_{n,0}$ is an initial phase offset, $\varsigma_n$ is a colored phase noise process, and $w_n(t)$ is the added white Gaussian receiver noise [16, Chapter 13.3]. The propagation delay $\tau_n$ from the satellite to node $n$ is rooted in the geometrical disposition of the two, where $\vec{x}_{\mathrm{sat}}$ and $\vec{x}_n$ are the geometrical position vectors of the emitting satellite and node $n$ respectively, $\|\cdot\|$ is the Euclidean vector norm, and $\mathrm{c}_0$ is the speed of light.

When this signal is digitized, the sample time instances are linked to the local time frame. We introduce a mathematical model to link the local clock readout value to the global time frame:

$$t = \mathcal{T}_n(t^\ell) \tag{4}$$

Using this notation, the local clock value of $t^\ell$ can be mapped to a global time stamp $t$ through the $\mathcal{T}_n$ operator, whose realization is different for each node $n$. A typical assumption is to model the time drift of a local clock with a linear relationship

$$\mathcal{T}_n(t^\ell) = \frac{t^\ell}{a_n} + \delta_n \,. \tag{5}$$

In this work, we will stick to that model above, and restrict the validity of $a_n$ and $\delta_n$ to a single pulsed acquisition interval (PAI) and allow them to change between the pulse-repetition interval (PRI). As is given in (1) $a_n$ is on average 1. As a first order assumption, we assume the correct clock rate, which does not need to be corrected during a single PAI as the acquisition record time is usually short (in the order of 10 µs to 100 µs). It should be noted, that any sufficient stable clock could be used in this scheme, it is not dependent on GNSS itself. Rather, a rough pre-synchronization is required, which fulfils the aforementioned assumption and enables sufficient alignment of the recording windows. However, the PRI is at least one order of magnitude larger and thus short term drifts become detectable in the form of a changing time offset. Meaning, this work uses the following assumption for a local clock to time transfer model

$$\mathcal{T}_n(t^\ell) = t^\ell + \delta_n\,[p] \quad \text{with } p = \left(t^\ell - t_0^\ell\right) \bmod \mathrm{PRI}\,, \tag{6}$$

where the pulse number $p$ can be obtained by an equidistant sampling of local time with the PRI offset to the start of a measurement at local clock value $t_0^\ell$.

With this formulation, the received signal (3) is translated into the receiver's time frame, yielding

$$\begin{aligned} r_n\left(t^\ell\right) = \quad & D_n \cdot s_{\mathrm{TV}}\left(t^\ell + \delta_n[p] - \tau_n\right) \\ & \exp\Big( - \mathrm{j}\left(2\pi f_{n,\mathrm{LO}} t^\ell + 2\pi f_{n,\mathrm{LO}} \delta_n[p] + \right. \\ & \left. \varphi_{n,0} + \varsigma_n(t^\ell + \delta_n[p])\right)\Big) + w_n(t^\ell + \delta_n[p])\,. \end{aligned} \tag{7}$$

To now obtain the synchronization parameters of the system, the goal is to obtain the relative time and phase differences between the base station (where the radar transmitter is colocated) and the remote nodes. This can be achieved in two sequential steps.

Firstly, between the received signal vector $r_0(t^\ell)$ of the base station and the remote nodes, a time offset $\Delta\hat{t}_{n\to 0}$ can be obtained. As is shown in [5], this can be achieved by a cross correlation and a nonlinear least squares (NLLS) approach with a sinc function kernel. The resulting time shift, denoted with $\Delta\hat{t}_{n\to 0}$ now contains the total time delay between both signal vectors. As communication systems aim for an optimal bandwidth efficiency and scrambling mechanisms are used, the signal from (3) should behave pseudo random and thus have a distinct peak in the cross correlation function suitable for NLLS peak finding [17, Chapter 2.3]. The exact shape of the cross-correlation function is determined by the occupied instantaneous bandwidth of the TV signal, however for peak-finding, the rough first order simplification of a sinc-shaped peak holds.

After the estimation of the time offset between the two broadcast signals, the received signal vector of the remote nodes can be shifted and interpolated in time, such that the received vectors of the remote signal and the base signal overlap in time to a subsample accuracy. If the estimation is unbiased, one can assume that

$$\delta_0[p] - \tau_0 = \delta_n[p] - \tau_n - \Delta\hat{t}_{n\to 0}[p] \tag{8}$$

holds.

This allows for the elimination of the signal's payload and LO carrier phase estimation. Under the assumption of a sufficiently high SNR ($D \cdot |s_{\mathrm{TV}}| \gg |w_n|$), an elementwise complex conjugate multiplication creates the phase difference and eliminates the modulation signal $m(t)$ as can be seen in (9), as $\angle\{x \cdot x^*\} = 0$ holds for any $x \in \mathbb{C}$. The contributing phase of the satellite TV signal is thus removed to zero, and only the LO phase differences remain. Taking a closer look at (9), one can see that the remaining phase is composed of a frequency offset $f_{n,\mathrm{LO}} - f_{0,\mathrm{LO}}$, a phase difference due to the clock offsets and time shifts, an additional phase offset, an initial random phase offset and two random phase noise processes. If one assumes that the LO frequency is referenced to the GNSS-disciplined reference oscillator, the frequency offset can be assumed to be zero. Although it might not hold for the instantaneous oscillator frequency, the frequency offset is usually sufficiently small (we have observed instantaneous frequency offsets in the range of up to 2 Hz to 5 Hz at 11 GHz PLL output frequency) such that the phase ramp is slow enough that it can be assumed as a constant in the PAI. Resulting of the previously mentioned

$$\begin{aligned} \angle\left\{r_0(t^\ell) \cdot r_n^*(t^\ell - \Delta\hat{t}_{n\to 0}[p])\right\} \simeq \angle\big\{ & s_{\mathrm{TV}}(t^\ell + \delta_0[p] - \tau_0) \cdot s_{\mathrm{TV}}^*(t^\ell + \delta_n[p] - \tau_n - \Delta\hat{t}_{n\to 0}[p])\big\} \\ & - \left(2\pi f_{0,\mathrm{LO}} t^\ell + 2\pi f_{0,\mathrm{LO}} \delta_0[p] + \varphi_{0,0} + \varsigma_0(t^\ell + \delta_0[p])\right) \\ & + \left(2\pi f_{n,\mathrm{LO}} t^\ell + 2\pi f_{n,\mathrm{LO}} \delta_n[p] + \varphi_{n,0} + \varsigma_n(t^\ell + \delta_0[p] - \Delta\hat{t}_{n\to 0}[p])\right. \\ & \left. - 2\pi f_{n,\mathrm{LO}} \Delta\hat{t}_{n\to 0}[p]\right) \end{aligned} \tag{9}$$

simplification, the difference phase from (9) resides (within a PAI) to a constant phase term superimposed with phase noise contributions, which only result from the LO signals used at the base and remote station.

The final phase estimation can be done with

$$\Delta\hat{\varphi}_n\,[p] = \angle\left\{\sum_{k'\in\mathcal{K}_p} r_0[k']\cdot r^*_{n,\leftrightarrow}[k']\right\}\,, \tag{10}$$

where $r_0[\cdot]$ is the sampled TV signal at the base station, and $r^*_{n,\leftrightarrow}[\cdot]$ is the complex-conjugate sampled TV signal at the remote station $n$ shifted in time by $-\Delta\hat{t}_{n\to 0}[p]$. The PAI comprises $K$ samples of which the set of samples within PAI number $p$ are denoted with $\mathcal{K}_p$.

### B. Correction of the radar data

Once the correction factors of $\Delta\hat{t}_{n\to 0}[p]$ and $\Delta\hat{\varphi}_n\,[p]$ have been obtained, they can be applied to the radar data channels of remote nodes $n$. As the geostationary satellite can be assumed to be stationary during a coherent processing interval (CPI), the time offset $\Delta\hat{t}_{n\to 0}[p]$ consisting of the clock offsets $\delta_n[p]-\delta_0[p]$ and the propagation delay differences $\tau_n - \tau_0$ is only changing because of the changing time offsets, as

$$\tau_n - \tau_0 = \text{const.} \tag{11}$$

holds during a CPI of a few dozen seconds [18]. Meaning, the constant time offset can be calibrated beforehand or obtained by range alignment methods [19]. Since the local clocks are pre-disciplined to GNSS (1) holds. Moreover, as long as the geometry remains stationary, i.e. (11) is valid, no additional drift is anticipated, and the synchronization is expected to remain time-invariant.

To obtain coherent radar channels, the received radar echo data of node $n$ can be shifted in time by $-\Delta\hat{t}_{n\to 0}[p]+\Delta t_{n,cal}$ and rotated in phase by $-\hat{\varphi}_n[p]$.

## III. Hardware Experiments

To validate the proposed synchronization scheme, an experimental hardware system was built. A total of two participating nodes were configured, each equipped with a GNSS-disciplined oscillator as the reference signal for the system clock and LO reference. Each node consists of a high performance RF system on a chip (SoC) sampling all channel at 5 GSPS. This way the total transponder bandwidth is available for synchronization, promising a high estimation precision [14, Chapter 3.11]. A basic linear frequency modulation (LFM) chirp signal was used in this experiment with a bandwidth of about 2.1 GHz and a duration of 25 µs. The PRI was set to 3.33 ms and the reception windows for both the satellite and radar echo receivers were configured to operate concurrently. The transmitted radar signal was received at both nodes after a true time-delay and thus allowing a method to obtain the estimation residuals, as ideally there should be no range and phase jitter remaining in the radar channel after correction and pulse-compression. The total receive window for the radar channel and the TV channel was 30 µs. For the receiving antennas two COTS 70 cm offset reflector antennas were used. As an initial test, a small separation of 2.60 m was configured. This first small baseline was chosen, as a rapid hardware setup was possible to serve as a proof-of-concept. A photo of the outdoor measurement setup can be seen in Fig. 2.

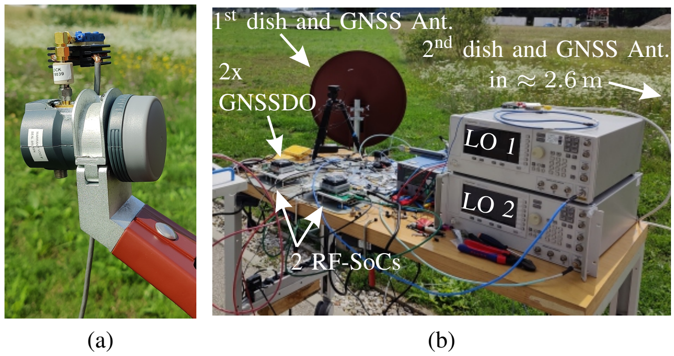


Fig. 2: Modified consumer LNB with the RF output port in (a) and a photo of the outdoor measurement setup in (b). Both nodes are operating independently using their own GNSS-disciplined oscillator.

### A. Modified consumer receiver hardware

The satellite TV broadcast signal provides a wide bandwidth pseudo-random high SNR waveform. Conventional low-cost LNBs at the feed point of a reflector antenna system are used by the public for broadcast reception and are also used in this demonstration. Those highly integrated devices contain a dual-polarization feed horn, low-noise amplifiers (LNAs) and a mixer for the intermediate frequency (IF) conversion, a PLL and oscillator for very low costs. In order to be able to use these devices for our application, a modification was necessary. There exist works that modify LNBs to accept an external reference frequency for the PLL such as [20], but as stated in II, only reference coupling is not enough for our application. In [21], it has also been shown that it is possible to directly inject the LO signal into consumer LNBs, but this would require less integrated LNBs than ours, and doing so would require additional cable routing.

The reverse-engineered block diagram illustrated in Fig. 3b was derived from the printed circuit board (PCB) in 3a. To access the RF signal, it can be tapped before entering the integrated circuit (IC) by removing the coupling capacitor and rerouting the signal to an output, which was achieved through a modified cover incorporating a SMA connector, where the center pin is press-fitted against the signal trace. This modified LNB can be seen in Fig. 2a. The resulting power spectral density (PSD) at the analog-to-digital converter (ADC) of the receivers can be seen in Fig. 4. After noise power calibration, the total signal power can be integrated over the used bandwidth, and thus a sufficient SNR of 9.3 dB at the base node and 20.4 dB at remote node is detected. The difference can be explained by different amplifiers after the LNBs as well as differently well realized RF transitions in the modified LNBs.

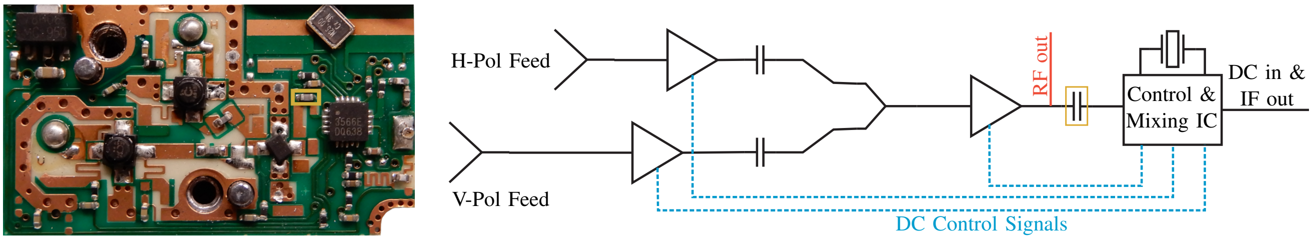


Fig. 3: Photo of the consumer LNB PCB in (a), where the removed capacitor is marked in yellow, and the simplified reverse engineered block diagram in (b), where the DC feeding networks have been simplified to control lines. The removed coupling capacitor and added output line have been marked in yellow and red respectively.

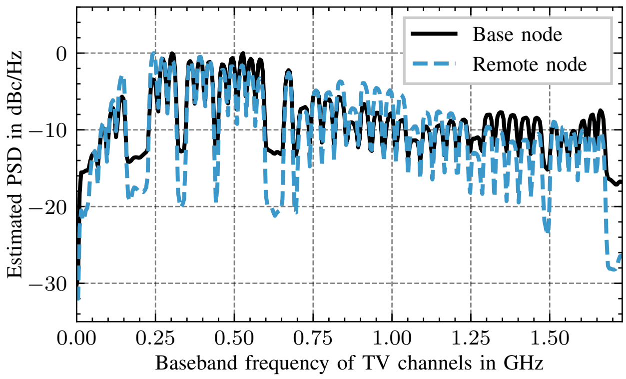


Fig. 4: Estimated PSD of the satellite TV receive channels using the modified consumer LNBs in horizontal polarization mode.

## IV. Discussion

Fig. 5 shows time and phase estimates obtained by the ASTRA broadcast signal. As expected, our two systems drifted in their local timing apart by more than 1.5 ns, resulting in a radar range drift of more than 22 cm in a CPI of just 20 s. In an intended system with a resolution in the single-digit centimeter regime, this drift is unacceptable if not corrected. Furthermore, a phase drift spanning multiples of $2\pi$ can be seen. There is no coherent image generation to be expected from this result, if not corrected. It is evident, that only oscillator disciplining via GNSS is not accurate enough for coherent radar operation in X band.

To validate, that the synchronization estimates by the broadcast signal coincide with the same drifts seen in the radar data, those can be applied to the true-time delayed radar signal before range-compression. Then a range estimate can be obtained by again a NLLS fit with a sinc kernel and the phase at the peak of the range compressed signal can be evaluated. Those can be seen in Fig. 6, where both the timing and phase residuals are shown. The $1\sigma$ timing deviation is observed at 2.42 ps and the $1\sigma$ phase deviation is observed at 1.69°. As can be seen, the residuals are drift-free and exhibit a low deviation, although the residuals seem to exhibit almost periodic behavior. The cause of this is yet unknown and will be investigated in the future. A range estimation deviation of 363 µm can be observed.

This result confirms the assumption of a stationary scenario for short CPIs, although it needs further investigation as a larger baseline distance increases the sensitivity to satellite motion. However, as the residuals clearly do not show white Gaussian behavior, there is more than just noise present in the residuals. Further investigations are needed to clarify the cause of them. If the obtained residuals were to show Gaussian noise behavior, a lower timing and phase deviation would be expected, however even current results already satisfy our requirements for coherent operation.

## V. Conclusion & Outlook

To summarize, the measurement results shown here serve as a proof-of-concept for ongoing developments in the next generation experimental system development. As they are obtained used comparatively small baselines, further studies need to be conducted to quantify the coherence possibilities for true far baseline sychonistation, which will be conducted in the coming years. With the usage of low-cost consumer receiver hardware, we can adopt this scheme to a multitude of participating nodes, as the RF SoC hardware employed in this scheme is already available for the radar task itself.

We have demonstrated a synchronization scheme that improves conventional GNSS-based timing by exploiting NC signal reception at the participating nodes. It is also thinkable to operate this scheme in a GNSS-denied scenario, as long as the signal of opportunity is present and the station's clocks are stable enough for record time window alignment. This allows large baseline radar operation for high-resolution imaging tasks while maintaining phase coherence. Without any real-time capable communication link between the nodes, this scheme is suitable for sparsely populated far baseline systems, which are investigated as part of the IoSiS-NG project (Imaging of Satellites in Space – Next Generation).

## Acknowledgment

This presented synchronization scheme is a part of a patent application filed with the German Patent and Trade Mark Office (Application No. 10 2025 124 272.0).

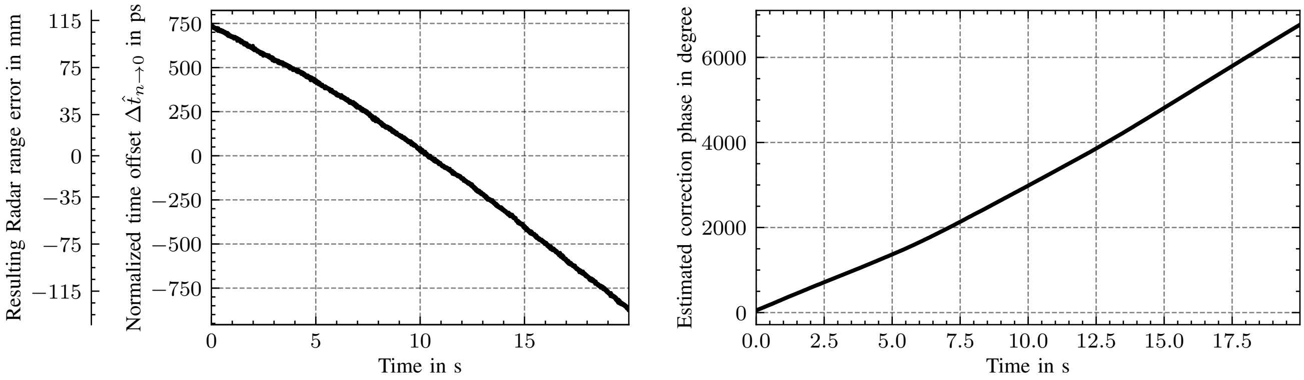


(a) (b)

Fig. 5: Timing and phase estimates obtained by the satellite TV signal with the timing and resulting range drift in (a) and the unwrapped estimated phase drift $\Delta\hat{\varphi}_n$ in (b). In (a) the median of 31.79 ns the of dataset was removed to clearly show the drift.

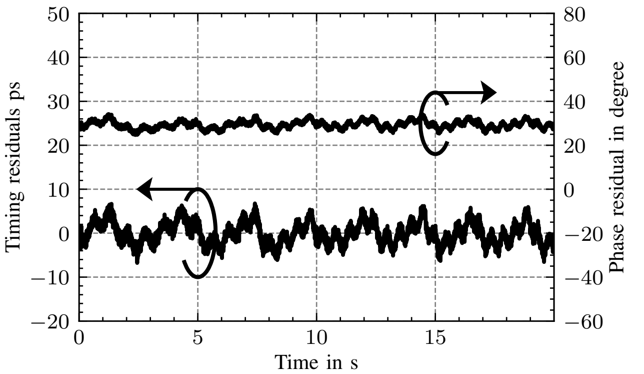


Fig. 6: Timing and phase residuals obtained via the radar receiver after the correction based on the NC signal processing has been applied. The mean phase residuals remain not at 0, because the calibration was done without true time-delay in the radar path.

## REFERENCES

[1] G. Krieger and A. Moreira, "Multistatic sar satellite formations: Potentials and challenges," in *Proceedings. 2005 IEEE International Geoscience and Remote Sensing Symposium, 2005. IGARSS '05.*, vol. 4. Seoul, Korea: IEEE, 2005, pp. 2680–2684.

[2] M. Villano, M. N. Peixoto, S. Kim, V. M. Pérez, N. Ustalli, J. Mittermayer, T. Börner, G. Krieger, and A. Moreira, "Potential of Multi-Static SAR Systems for Earth Monitoring and Their Demonstration Using Swarms of Drones," in *IGARSS 2023 - 2023 IEEE International Geoscience and Remote Sensing Symposium*, Jul. 2023, pp. 4586–4589.

[3] S. Dunkel and E. Schreiber, "Phase Synchronization Concept for the Bistatic Extension of the Airborne F-SAR System," in *2024 Kleinheubach Conference*, Sep. 2024, pp. 1–4.

[4] J. Kanz, C. Bonfert, C. Gesell, A. Grathwohl, F. Bormuth, G. Krieger, and C. Waldschmidt, "Coherent Multistatic UAV-Based SAR," *IEEE Transactions on Radar Systems*, pp. 1–1, 2025.

[5] S. Prager, M. S. Haynes, and M. Moghaddam, "Wireless Subnanosecond RF Synchronization for Distributed Ultrawideband Software-Defined Radar Networks," *IEEE Transactions on Microwave Theory and Techniques*, vol. 68, no. 11, pp. 4787–4804, Nov. 2020.

[6] R. H. Kenney, J. G. Metcalf, and J. W. McDaniel, "Wireless Distributed Frequency and Phase Synchronization for Mobile Platforms in Cooperative Digital Radar Networks," *IEEE Transactions on Radar Systems*, vol. 2, pp. 268–287, 2024.

[7] Y. Chen, D. Liang, H. Yue, D. Liu, X. Wu, H. Zhang, Y. Jiao, K. Liu, and R. Wang, "Implementation of a Phase Synchronization Scheme Based on Pulsed Signal at Carrier Frequency for Bistatic SAR," *Sensors*, vol. 20, no. 11, p. 3188, Jan. 2020.

[8] S. Anger, M. Jirousek, S. Dill, and M. Peichl, "High-resolution radar imaging of space objects," in *Advanced Maui Optical and Space Surveillance Technologies Conference (AMOS)*, Maui, Hawaii, Sep. 2024.

[9] "Our Coverage | SES — ses.com," https://www.ses.com/our-coverage#/explore/orbital-position/196, accessed 2025-09-15.

[10] T. Žuntar, E. Busley, J. Borgmann, and M. Krist, "Time Synchronization via TDoA Measurement of Broadband Satellite Signals in L-, X- and Ku-Band," in *2024 21st European Radar Conference (EuRAD)*, Sep. 2024, pp. 184–187.

[11] E. Busley, T. Žuntar, J. Borgmann, and M. Krist, "Time transfer via single-record TDoA measurements of GNSS satellites using direct cross-correlation and relative pilot code phases," *IET Radar, Sonar & Navigation*, vol. 18, no. 12, pp. 2447–2453, 2024.

[12] O. Jean and A. J. Weiss, "Passive Localization and Synchronization Using Arbitrary Signals," *IEEE Transactions on Signal Processing*, vol. 62, no. 8, pp. 2143–2150, Apr. 2014.

[13] J. S. Picard, "Exploiting Signals-of-Opportunity for the Synchronization of Moving Sensors," in *2018 IEEE 19th International Workshop on Signal Processing Advances in Wireless Communications (SPAWC)*, Jun. 2018, pp. 1–5.

[14] S. M. Kay, *Fundamentals of Statistical Signal Processing. 1: Estimation Theory*, 20th ed. Upper Saddle River, NJ: Prentice Hall PTR, 2013.

[15] K. Weiss, A. Lisowiec, and W. Steplewski, "Limit parameters of GPS disciplined quartz frequency sources," in *Proceedings of CAOL'2003. (IEEE Cat. No.03EX715)*, vol. 2, Sep. 2003, pp. 262–264 vol.2.

[16] D. M. Pozar, *Microwave Engineering*, 4th ed. Hoboken, NJ: Wiley, 2012.

[17] H.-J. Zepernick and A. Finger, *Pseudo Random Signal Processing: Theory and Application*. Chichester, England Hoboken, NJ: Wiley, 2005.

[18] F. Bushuev, M. Kaliuzhnyi, Y. Sybiryakova, O. Shulga, S. Moskalenko, O. Balagura, and V. Kulishenko, "Results of the Ongoing Monitoring of the Position of a Geostationary Telecommunication Satellite by the Method of Spatially Separated Basis Receiving of Digital Satellite Television Signals," *Latvian Journal of Physics and Technical Sciences*, vol. 53, no. 5, pp. 5–16, Oct. 2016.

[19] M. Rodriguez-Cassola, P. Prats-Iraola, P. Lopez-Dekker, A. Reigber, G. Krieger, and A. Moreira, "Autonomous time and phase calibration of spaceborne bistatic SAR systems," in *EUSAR 2014; 10th European Conference on Synthetic Aperture Radar*, Jun. 2014, pp. 1–4.

[20] D. E. Herrera, A. F. Saez, and L. Dauvin, "Low-cost Ku band interferometer for educational purposes," in *Millimeter, Submillimeter, and Far-Infrared Detectors and Instrumentation for Astronomy VIII*, vol. 9914. SPIE, Jul. 2016, pp. 880–895.

[21] N. A. Salmon, P. N. Wilkinson, and J. Radiven, "Amplitude and intensity interferometry using satellite LNB receivers for innovative and low cost microwave and millimetre wave sensor development," in *Millimetre Wave and Terahertz Sensors and Technology V*, vol. 8544. SPIE, Oct. 2012, pp. 80–89.